Image analysis of 3-D clouds of bubbles

C. VIGNEAULT[1], B. PANNETON[1] and G.S.V. RAGHAVAN[2]

[1]Agriculture Canada Research Station, St-Jean-sur-Richelieu, PQ, Canada J3B 3E6; [2]Agricultural Engineering Department, Macdonald Campus of McGill University, Ste-Anne de Bellevue, PQ, Canada H9X 3V9. *[1]Contribution Number: 335/92.06.02R. Received 10 October 1991; accepted 2 October 1992.*

Vigneault, C., Panneton, B. and Raghavan, G.S.V. 1992. **Image analysis of 3-D clouds of bubbles**. Can. Agric. Eng. **34**:347-352.
Recently, novel techniques have been experimented for the measurement of bubble parameters. However, image analysis remains a very attractive approach. The main drawback of this technique is the error generated by the effect of the offset distance between the bubble position and the plane of best focus (object plane). A discriminatory parameter has been developed to permit the measurement of spherical equivalent diameter of bubbles in a 3-D system. The relationship between the error on the measurement of the spherical equivalent diameter of the bubble and the discriminatory parameter was determined. The depth of field of view where the measurements can be performed was established. Two bubble generators were characterized using the discriminatory parameter along with the technique of bubble measurement.

Même s'il existe de nouvelles méthodes de mesure du diamètre de bulles, l'analyse d'image demeure toujours une méthode très intéressante. Le principal désavantage de cette dernière est l'erreur de mesure due à la distance entre le plan de la bulle et le plan du meilleur foyer (plan de l'objet). L'élaboration d'un paramètre discriminatoire a permis de mesurer le diamètre équivalent de bulles dans un système en trois dimensions. L'erreur faites lors de la mesure du diamètre des bulles a été évaluée en fonction du paramètre discriminatoire. La profondeur de champs où les mesures peuvent être faites a été déterminée. L'utilisation de ce paramètre a également permis la caractérisation de la population de bulles générées par deux types de générateur.

INTRODUCTION

There is a wide range of operations and processes in industry and pollution control in which gas, as a dispersed phase, plays an important role such as the fermentation process or aeration pool. For many industrial bubble generators, the bubbles generated are of variable size. The determination of the bubble size and motion is helpful in determining the efficiency of the bubble generator with respect to its intended application.

The mechanism of bubble formation has been a subject of interest for several decades (Hadamard 1911). The main research tool used for determining the bubble velocity was measurement of bubble position on two successive photographs. Usually the bubble size was determined by measuring the liquid displaced by a given number of bubbles (Haberman and Morton 1953).

Tsukada and Horio (1990) presented novel techniques recently developed for the measurement of bubble parameters. They classified the image analysis as one of the best. The development of real-time digital image analysis has permitted the measurement of key bubble parameters in a two-dimensional bed (Lim et al. 1990). To avoid field depth effect, Lim et al. (1990) built their fluidized bed from a 9 mm deep aquarium and positioned its centre in the field of view of a camera. The drawbacks of this technique were the wall effects and the restriction of the dispersion of the bubbles to only two dimensions.

Vigneault et al. (1990) developed an image analysis system for the determination of the volume, the equivalent spherical diameter, and the vertical velocity of gas bubbles formed at the tip of a circular orifice submersed in water. With this single bubble image analysis technique, the image taken by the camera was focused on the vertical axis of the orifice and gave accurate measurements of the volume and vertical speed of the bubbles. However, when a cloud of bubbles is generated in a 3-D space, a discriminatory parameter must be established in order to define a depth of field where measurements can be performed, while keeping accuracy within known limits.

The first objective of this research was to develop a discriminatory parameter required for the characterization of a cloud of bubbles in a 3-D system and evaluate the application of this parameter to bubble sizes varying from 0.5 to 3.5 mm in diameter. The second objective was to evaluate the performance of the image analysis system applied to a 3-D system, by measuring the size of bubbles generated as well as the air flow rate produced by two different sintered stainless steel filters, so called diffusers, having pore sizes of 0.5 and 2 μm in diameter.

MATERIALS AND METHODS

The image analysis system was described in detail by Vigneault et al. (1990). With the vision system, the images were captured by an electronic camera which produced a video signal and transferred it to a digitizing board. The digitized images were then displayed in real time on a monitor. Up to four images could be stored in memory for further analysis. The chosen lens resulted in a pixel size of 25 μm.

Discriminatory parameter

When using a fixed capillary tube for bubble generation, the distance between the camera and the tip of the tube could be adjusted to obtain well-focused images of bubbles. The plot of gray levels versus pixel position on a horizontal line across the centre of a bubble shows a slope with a sharp drop at the edges of the bubble (Fig. 1). The slope at the bubble boundary decreases as the field of view of the camera is moved away

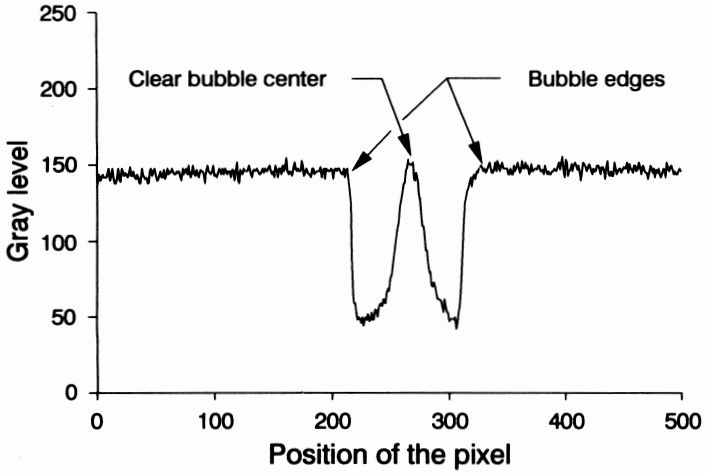

Fig. 1. Gray level along a horizontal line centered on a bubble.

from the capillary tube. The slope can be used as a parameter to discriminate between in focus and out of focus bubbles, provided that one can define a range of slope magnitude over which the sizing accuracy is acceptable. To evaluate the relationship between the slope and the accuracy of the bubble size, the slope and the bubble equivalent spherical diameter, D_s, were measured for bubbles of known sizes. Measurements were made with bubbles randomly placed within 10 mm on either side of the plane of best focus. Bubbles of known sizes were generated using the technique described in Vigneault et al. (1992). The slope was evaluated around X_{min} and X_{max} over a horizontal length of 11 pixels (Fig. 2) resulting in 22 measurements. The maximum slope measured was used as the discriminatory parameter. The X_{min} and X_{max} values were defined as the minimum and the maximum values of the X coordinate of the contour pixels of a bubble. Plotting D_s as a function of the maximum slope showed how the measurement accuracy degrades as the maximum slope decreases. The measurements were performed using four equivalent spherical diameters of bubbles; 3.35 mm, 2.29 mm, 1.40 mm, and 0.74 mm. For each bubble size, two hundred bubbles were analyzed.

Depth of field

The depth of field (DOF) is the sum of the offset distance fore and aft from the object plane over which an acceptable sizing accuracy is retained. After knowing the minimum value of the maximum slope for acceptable accuracy, the DOF was measured by moving a bubble attached to a capillary tube fore and aft of the object plane, in 1 mm increments until the minimum value of the maximum slope was reached. Bubbles ranging from 0.75 to 3.25 mm in equivalent spherical diameter were used and 50 replications were made at each bubble size. Plots of the maximum slope as a function of the offset from the object plane were used to define the DOF.

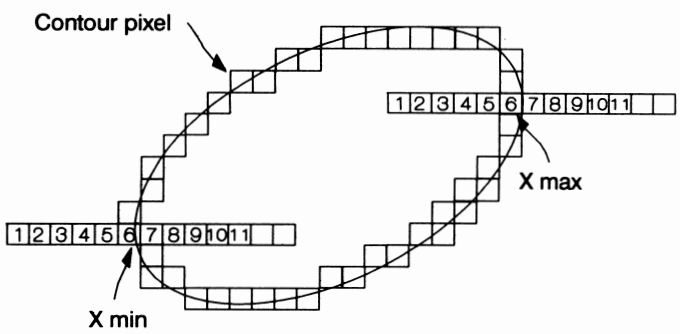

Fig. 2. Digitized bubble contour and locations for computing the maximum slope.

Gas flow rate and bubble size distribution

Once the DOF was defined, the gas flow rate and the bubble size distribution of two bubble generators (sintered stainless steel diffusers with 0.5 and 2.0 μm pore size) were measured. The measurement was achieved by looking at a horizontal slice of the bubble cloud covering the entire cross section of the cloud. The slice was divided into cubes with a side length equal to the DOF (Fig. 3). The width and height of the cubes could be made larger or smaller if desired, by adjusting the active portion of the camera field of view.

For each cube, the camera was positioned such that the object plane was in the middle the cube. At each measurement point, twenty images were captured and analyzed. The analysis proceeded in three steps. First, the objects were identified by thresholding the image. The contour was traced and the maximum slope was calculated for each object. Secondly, the objects were classified. Objects with a maximum slope smaller than the minimum value of the maximum slope defining the DOF were classified as object out of focus (OOFO). Other objects were presented to the operator who had to decide how many bubble shadows created an object. When only one bubble (OOB) was identified, its volume and D_s were computed. If more than one bubble was identified for an object, the number of grouped bubbles was stored for further use. Finally, a bubble size distribution and a gas flow rate were computed. The bubble size distribution was built from OOB data and then corrected to account for the grouped bubbles and for the possibility that large objects were hiding smaller ones directly in front of or behind them. The correc-

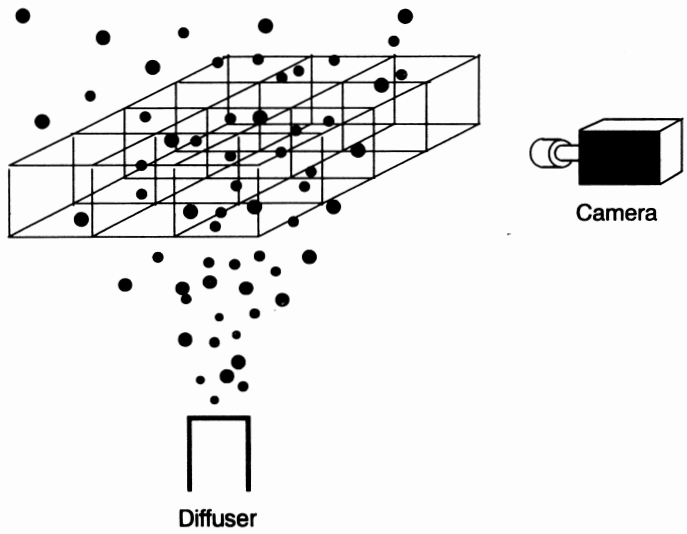

Fig. 3. Bubble cloud sampling.

tion for grouped bubbles was achieved as:

$$N'_i = \frac{N_i}{\sum_{i=1}^{n} OOB} N_T \quad (1)$$

where:

N_i' = number of bubbles in class i corrected to account for grouped bubbles,

N_i =number of bubbles in class i determined from OOB,

$\sum_{i=1}^{n} OOB$ = sum of bubbles in all classes determined from OOB,

N_T = sum of bubbles in all classes including OOB and grouped bubbles, and

n = number of classes.

The correction to account for the possibility that large objects were hiding smaller ones was performed using:

$$N''_i = \frac{N'_i V_t}{V_t - V_{Hi}} \quad (2)$$

where:

N_i'' = number of bubbles in class i corrected to account for grouped bubbles and for possibility of hidden bubbles,

V_t = total volume of the sample (μL), and

V_{Hi} = volume of bubble of class i which could be hidden (μL).

The V_{Hi} was calculated as:

$$V_{Hi} = \frac{\pi}{4} \sum_{j=1}^{n} (DOF - D_{sj}) (D_{sj} - D_{si})^2 N'_j \quad (3)$$

where:

DOF = depth of sample (mm),

D_{si}, D_{sj} = mean diameter of classes i and j respectively (mm), and

N_j' = number of bubbles in class j corrected to account for grouped bubbles.

The results obtained from the cubic samples were assembled into a single number distribution. Then, for each class, the volume fraction was computed as:

$$R_i = \frac{N''_i V_i v_i}{20 Q H} \quad (4)$$

where:

$$Q = \frac{1}{20 H} \sum_{i=1}^{n} N''_i V_i v_i \quad (5)$$

and

R_i =volume fraction in class i,

V_i = mean volume of bubbles in class i (μL),

v_i = vertical speed of bubbles in class i (mm•s^{-1}),

H = height at which cubic samples taken (mm), and

Q = gas flow rate (μL•s^{-1}).

The vertical speed of the bubbles was determined using the empirical Eqs. 6 and 7 reported in Vigneault et al. (1992) for a cloud of air bubbles in tap water:

$$\ln (v_t) = 1.21 + 8.48D - 5.52D^2 + 1.51D^3 - 0.15D^4, \quad \text{for } D < 1.3\text{mm} \quad (6)$$

$$v_t = 348.71 - 14.73D, \quad \text{for } 1.3\text{mm} \le D \le 4.0\text{mm}$$

where:

v_t = equilibrium rising velocity of air bubble with respect to ambient water (mm•s^{-1}), and

D = equivalent spherical bubble diameter (mm).

In the case of high air flow rates, the water is entrained by the bubble cloud. Therefore, the velocity of the bubble with respect to the camera frame of reference is the sum of v_t and the liquid velocity. Measurement of water velocity was performed at each measurement point. It was achieved by measuring the velocity of five bubbles by the camera system using the same method as that described by Vigneault et al. (1992). The mean vertical liquid speed was taken to be the average of the differences between the measured bubble speed and v_t.

An independent measurement of gas flow rate was used for comparison purposes. A volume displacement method was used where a water-filled graduated cylinder was positioned to capture the whole bubble flux. The time required to capture 10 mL of air was measured with a stopwatch. Given a total reaction time of 0.5 s, the accuracy of this method was better than 1%.

RESULTS AND DISCUSSION

Discriminatory parameter

Figure 4 shows the variation of the measured D_s with the maximum slope at equivalent spherical diameters of bubbles of 3.35 mm, 2.29 mm, 1.40 mm, and 0.74 mm. The precision in the measurement of the spherical equivalent diameter of the bubble was related to the maximum slope. The greatest fluctuations in all cases were seen for maximum slopes less than about 15. Furthermore, all the curves showed a significant slope change at a maximum slope value of about 15, indicating a rapid increase of the error on the measurement of the spherical equivalent diameter of the bubble with a decreasing maximum slope. Table I shows the R^2 and the equations of the curves fitted to the data in Fig. 4. The constant term on the right-hand side of the equations in Table I is equal to the nominal spherical equivalent diameter of the bubble. Thus the other term presents the systematic error associated with a given maximum slope. Figure 5 is a plot of this error term. An error associated with a maximum slope larger than 15 is considered acceptable since it is equivalent to the size of two pixels or an error of about 50 μm on the equivalent spherical diameter. On Fig. 5, it can be seen that

the magnitude of the error term is approximately constant over the range of bubble size considered for a maximum slope larger than 15. Therefore, a single equation can be written for the error term that can be used to correct the measured bubble D_s. Equation 8 was obtained by least square fit of the data of the maximum slope in gray level (ms) in Fig. 5 for $ms \geq 15$:

$$\varepsilon = 1.062 \exp(-0.216\, ms), \quad \text{for } ms \geq 15, \tag{8}$$

where:

ε = error on Ds (mm), and

ms = maximum slope of gray level.

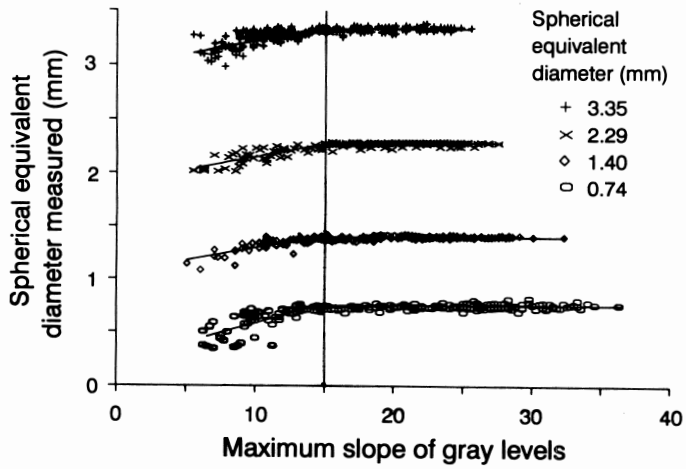

Fig. 4. Diameter variations for different bubble sizes as a function of the maximum slope.

Table I. Regression equations and R^2 of the curves presented in Fig. 4

Bubble diameter (mm)	Equation of D_s vs Maximum slope, ms	R^2
3.35	$D_s = 3.349 - 0.831\, e^{-0.19\, ms}$	0.64
2.29	$D_s = 2.286 - 0.588\, e^{-0.18\, ms}$	0.67
1.40	$D_s = 1.395 - 1.080\, e^{-0.24\, ms}$	0.82
0.74	$D_s = 0.743 - 1.750\, e^{-0.25\, ms}$	0.72

Depth of field

Figure 6 shows the maximum slope as a function of the offset from the object plane. At a maximum slope of 15, the average depth of field was 6.67 mm for all the spherical equivalent diameters of bubbles tested. A linear regression was performed on the depth of field measured at a maximum slope of 15 for all spherical equivalent diameters of the bubbles presented at Fig. 7. The regression gave a slope of 0.076 and an intercept of 6.519. A Students' t-distribution was performed and confirmed that the slope was not significantly different from zero ($t = 0.505$, $P = 0.632$). This indicated that the depth of the field as defined here is independent of the spherical equivalent diameter of the bubble. Therefore, the depth of the field was considered to be equal to 6.67 mm.

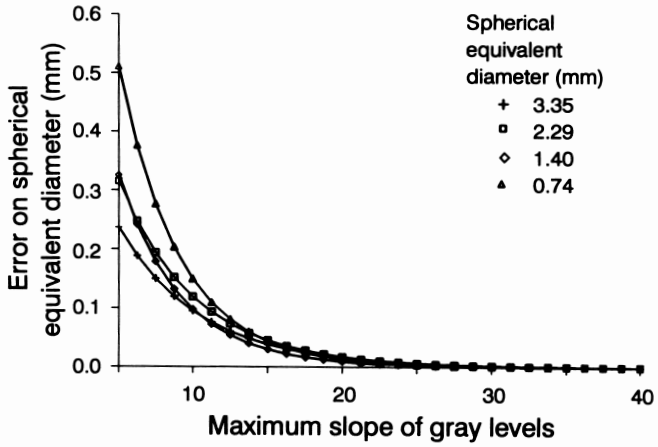

Fig. 5. Systematic error in spherical equivalent diameter of the bubble as a function of the maximum slope.

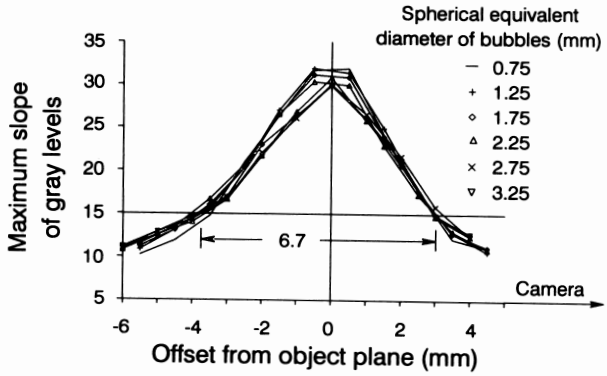

Fig. 6. Variation of the maximum slope with the offset from the object plane for spherical equivalent diameters of bubbles ranging from 0.75 to 3.25 mm.

From Fig. 6, it is noted that the degradation in the maximum slope is more gradual for negative offsets (closer to camera) with an acceptable offset of approximately 3.7 mm compared to approximately 3 mm on the opposite side.

Gas flow rate and bubble size distribution measurements

To obtain the real dimensions of the bubbles analyzed by the imaging system, the diameters were readjusted using Eq. 9 for the error term.

$$D_{sc} = D_s + \varepsilon \tag{9}$$

where:

D_{sc} =corrected spherical equivalent diameter (mm),

D_s =measured spherical equivalent diameter (mm), and

ε = error on D_s (mm).

The distributions of the two distinct populations obtained with the two diffusers are presented in Figs. 8 and 9. No published data or alternate method of measurements were available to check the accuracy of these distributions. It is

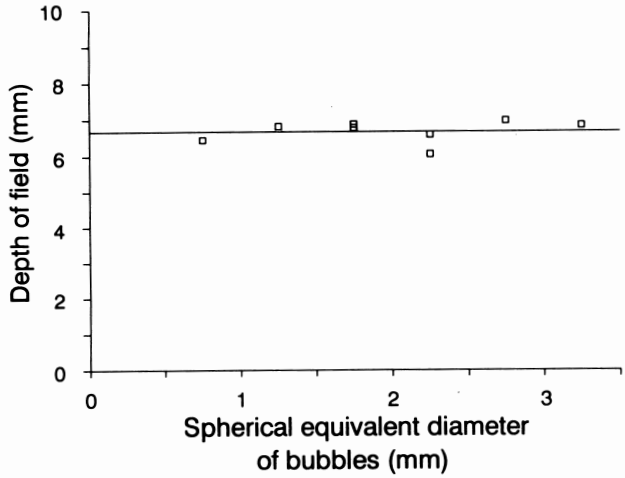

Fig. 7. Depth of field as a function of spherical equivalent diameters of the bubbles.

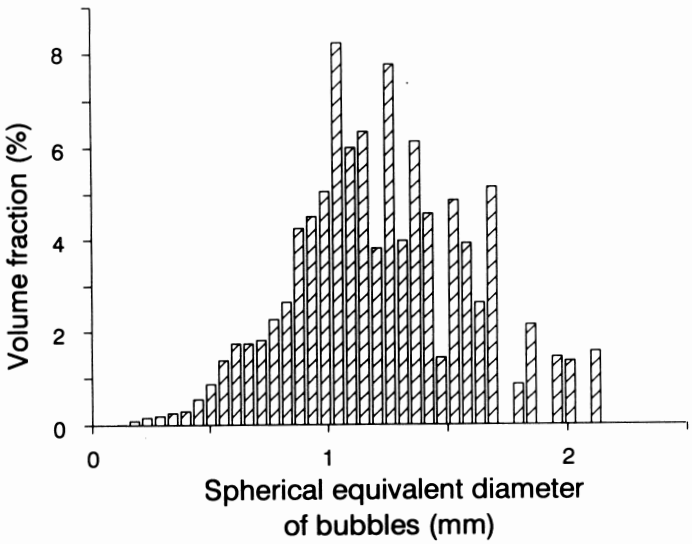

Fig. 8. Volume distribution for a 0.5 μm diffuser at 350 μL•s^{-1}.

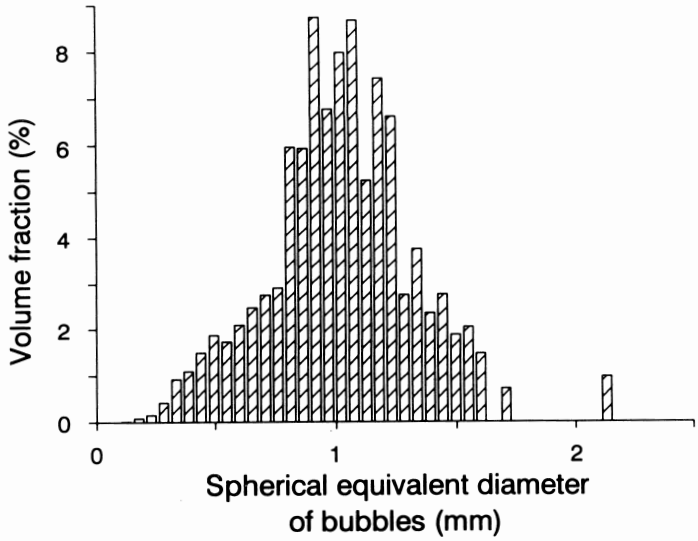

Fig. 9. Volume distribution for a 2 μm diffuser at 414 μL•s^{-1}.

interesting to note that both distributions are smoother in the small diameter range suggesting that these sintered metal diffusers tend to form small bubbles more regularly than larger ones. Also despite a large difference in pore sizes (0.5 versus 2.0 μm) and a small difference in flow rates (350.4 μL•s^{-1} for 0.5 μm and 414.8 μL•s^{-1} for 2 μm), both distributions have a peak at spherical equivalent diameters between 1.1 and 1.2 mm. Moreover, the distribution for the 0.5 μm diffuser is shifted towards larger diameters when compared to the one obtained with the 2.0 μm diffuser. This result suggests that coalescence of bubbles originating from adjacent pores dominates the process of bubble formation with these diffusers when the pore size becomes smaller resulting in a higher pore density.

Trials were conducted using higher air flow rates generating dense clouds of bubbles. The system did not successfully distinguish between the background and the bubble boundaries due to the great number of overlapping bubbles. These bubble populations were not characterized since the size distribution of the few individual bubbles analyzed was not

Table II.Flow rate comparisons

Diffuser pore size (μm)	Rep	Flow rate (μL•s^{-1}) Camera system Q_c	Flowmeter system Q_F	Difference $\frac{100 (Q_F - Q_c)}{Q_F}$ %	Mean of differences %
0.5	1	377	350	-7.9	
	2	301	351	14.2	
	3	347	351	1.2	
	4	290	352	17.6	
	5	323	348	7.2	6.5
2	1	348	413	15.7	
	2	311	408	23.8	
	3	365	423	13.8	17.7

representative of the real bubble size distribution. A maximum bubble surface projection of approximately 30% was found to be the limit for a successful population characterization but this is highly dependent on the bubble size.

Flow rates measured by the vision system and the water displacement method are compared in Table II. For sintered metal diffusers having orifices of 0.5 μm and 2 μm, the average flow rates were respectively 350.4 $\mu L \bullet s^{-1}$ and 414.8 $\mu L \bullet s^{-1}$. One should note that the vision system has generally underestimated the flow rate by up to 23.8% (Table II). No explanation could be put forward to justify this discrepancy. However, the agreement between the two methods of measurement was good, given the uncertainty of the bubble velocity as the diameter of the bubbles increases (Vigneault et al. 1992).

CONCLUSION

A discriminatory parameter required for the characterization of clouds of bubbles was developed by 3-D image analysis system. It was demonstrated that the discriminatory parameter, a minimum value of the maximum slope of 15, was independent of bubble size for the system under analysis. It permitted the determination of the depth of field and allowed the elimination of bubbles out of focus. With this discriminatory parameter, clouds of bubbles generated by two different diffusers were studied and the population distribution was determined. However, this system is limited to relatively low density bubble populations because it does not analyze the characteristics of overlapping bubbles in the images and it cannot "see" inside of a dense cloud.

ACKNOWLEDGEMENT

The authors gratefully acknowledge the funding by COR-PAQ of the Ministère de l'Agriculture, des Pêcheries et de l'Alimentation du Québec.

REFERENCES

Haberman, W.L. and R.K. Morton. 1953. An experimental investigation of the drag and shape of air bubbles rinsing in various liquids. Report 802. Navy Department, Washington, DC.

Hadamard, J. 1911. Mouvement permanent lent d'une sphère liquide et visqueuse dans un liquide visqueux. *Comptes rendus de l'Académie des sciences* (Paris, France) 152:1735-1738.

Lim, K.S., P.K. Agarwal and B.K. O'Neill. 1990. Measurement and modelling of bubble parameters in a two-dimensional gas-fluidized bed using image analysis. *Powder Technology* 60:159-171.

Tsukada, M. and M. Horio. 1990. Gas motion and bubble formation at the distributor of a fluidized bed. *Powder Technology* 63:60-74.

Vigneault, C., B. Panneton and G.S.V. Raghavan. 1990. Real-time image digitizing system applied to air bubble generator characterization. ASAE Paper No 90-3535. St. Joseph MI: ASAE.

Vigneault, C., B. Panneton and G.S.V. Raghavan. 1992. Real-time image digitizing system applied to air bubble measurement. *Canadian Agricultural Engineering* 34(2):151-155.